ACS Photonics
Article
pubs.acs.org/journal/apchd5

Experimental Demonstration of 4n^2 Classical Absorption Limit in Nanotextured Ultrathin Solar Cells with Dielectric Omnidirectional Back Reflector

Andrea Ingenito, Olindo Isabella, and Miro Zeman*

PVMD Laboratory, Delft University of Technology, Dimes, P.O. Box 5053, 2600 GB Delft, The Netherlands

ABSTRACT: The experimental demonstration of the 4n^2 classical absorption limit in solar cells has been elusive for the last 30 years. Especially the assumptions on front and internal rear reflectance in a slab of absorbing material are not easily fulfilled unless an appropriate light-trapping scheme is applied. We propose an advanced metal-free light-trapping scheme for crystalline silicon wafers. For different bulk thicknesses, at the front side of the wafers we applied a nanotexture known as black-silicon. At the rear side, we implemented a random pyramidal texture coated with a distributed Bragg reflector. Such a dielectric back reflector was designed to exhibit a maximized omnidirectional internal rear reflectance in the region of weak absorption of crystalline silicon. Integrating the measured absorptance spectra of our wafers with the reference solar photon flux between 400 and 1200 nm, we could calculate the so-called implied photogenerated current densities. For wafers thinner than 35 μm, we achieved more than 99% and up to 99.8% of the implied photogenerated current density based on the theoretical 4n^2 classical absorption limit. Successful implementation of our maskless and metal-free light-trapping scheme in crystalline silicon solar cells requires the adequate surface passivation of the front nanotexture. For this purpose we used thermal silicon oxide, but we discuss also the usage of aluminum oxide. Our findings, applied in a solar device structure where front side losses are minimized, open the way for the realization of next-generation high-efficiency, cost-effective, and ultrathin crystalline silicon solar cells.

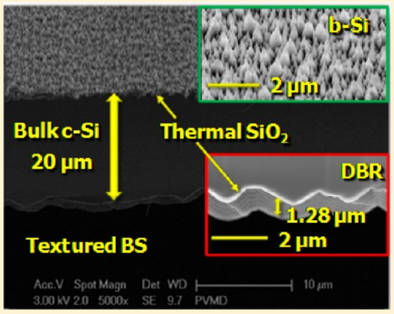

KEYWORDS: *black-silicon, light in-coupling, optical losses, Tiedje−Yablonovitch limit, Bragg reflector*

Light trapping using textured surfaces and metallic back reflector (BR) has contributed to a significant conversion efficiency gain in crystalline silicon (c-Si) solar cells.[1] For continuing large-scale implementation of c-Si solar cells, their production cost must be further lowered by optimizing manufacturing processes and by using fewer materials without sacrificing the efficiency.[2−4] Particularly, thinner wafers that are lighter and more flexible[5] show a lower bulk recombination[6] and exhibit, in the case of Czochralski wafers, a lower light-induced degradation.[7,8] However, as c-Si is an indirect band gap semiconductor, the absorption of the near-infrared region (NIR) of the solar spectrum is significantly reduced in thinner wafers. Thus light-trapping schemes are essential in thin c-Si solar cells,[9] where light management techniques such as front light in-coupling, light scattering, and internal back reflectance (R_b) have to be optimal and concurrently active. These techniques ultimately fulfill the ideal hypotheses of the so-called 4n^2 classical absorption limit in a dielectric slab,[10] where n is the real part of its complex refractive index: (i) a surface-textured morphology at the air/dielectric interface in the role of a perfect broad-band antireflective coating (ARC) (reflectance $R = 0\ \forall\lambda$), (ii) randomized and ideally diffused light inside the slab (the so-called Lambertian scattering), and (iii) a perfect back reflector ($R_b = 1\ \forall\lambda$). In the wavelength region of weak absorption of c-Si ($\alpha d < 1$), where α and d are the absorption coefficient and thickness of the dielectric slab, respectively, such a light-trapping scheme theoretically results in an absorption enhancement factor of 50.[11]

Light trapping in commercial c-Si solar cells is achieved by using random texturing and metal or a dielectric/metal stack as back reflector. Even though standard random pyramid texturing exhibits a nearly Lambertian scattering,[11,12] it does not result in a perfect broad-band antireflective effect. In this respect, nanotextures with feature sizes in the subwavelength range are considered valid candidates for providing a broad-band antireflective effect.[13] Among various advanced light-trapping schemes that were lately presented to fulfill the hypothesis of the 4n^2 classical absorption limit,[14−16] a recent optical simulation study showed that the absorptance in c-Si can approach the 4n^2 classical limit in a just 2 μm thick structured c-Si slab. Such a slab was endowed with high aspect ratio periodic nanogratings at the front side (FS) for antireflective purposes and with low aspect ratio pyramidal structures at the back side (BS) for efficient long-wavelength light scattering.[13] We call this arrangement decoupled front and rear texturization.[17] Based on this design, a c-Si solar cell with a thickness of around 9 μm was also reported to achieve a potential photogenerated current density (J_{PH}) > 36 mA/cm^2 and a conversion efficiency of >7%.[18]

Received: December 8, 2013
Published: February 13, 2014

dx.doi.org/10.1021/ph4001586 | *ACS Photonics* 2014, 1, 270−278

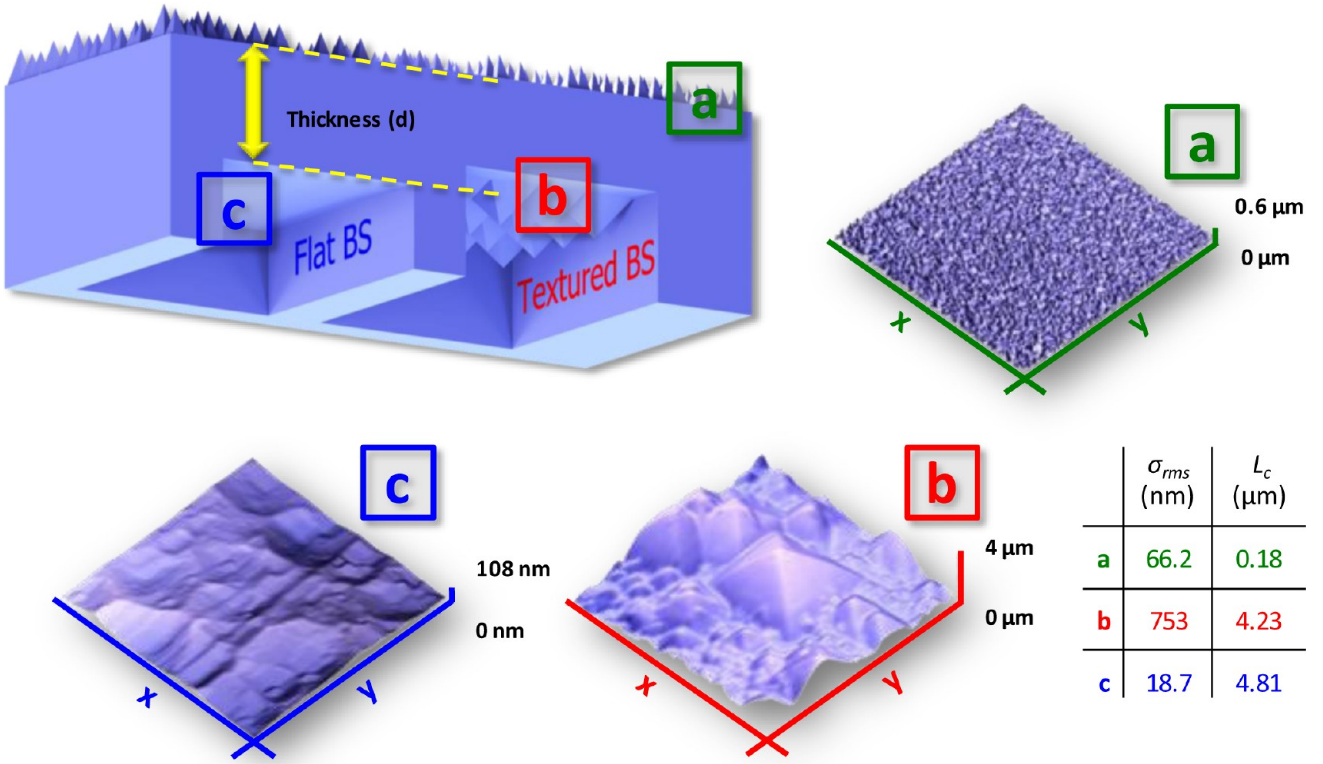

	σ_{rms} (nm)	L_c (µm)
a	66.2	0.18
b	753	4.23
c	18.7	4.81

Figure 1. (Top left) Schematic structure of our structured c-Si wafers: (a) nanotexture at the FS with (b) textured or (c) flat BS. Scale bars in *x*- and *y*-directions of the AFM scans are 20 μm long. In the inset table, AFM-extracted $\sigma_{\rm rms}$ and $L_{\rm c}$ are reported for the three investigated surfaces.

In this contribution we propose an advanced metal-free light-trapping scheme for crystalline silicon solar cells based on decoupled front and rear textures. Our scheme employs low-cost and industrially scalable processes, such as nanotexturing, also known as black-silicon (b-Si), at FS and random pyramids coated with a distributed Bragg reflector (DBR) at the BS.[19,20] In the following we shall report on our process flow and design steps for the realization of a dielectric omnidirectional BR. Afterward we shall present our measured c-Si absorptance spectra and compare the performance of dielectric and reference silver BRs with the $4n^2$ classical absorption limit. Finally, we shall discuss our vision of next-generation c-Si solar cells. In fact our front nanotexture can be efficiently passivated by using SiO_2 grown via dry thermal oxidation[21] or by Al_2O_3 deposited via atomic layer deposition (ALD).[22] Moreover, it has been also demonstrated that efficiencies comparable with state-of-the-art c-Si solar cells can be achieved by using front b-Si texture.[21] This opens the possibility to couple our advanced light-trapping scheme in ultrathin c-Si wafers with efficient passivation techniques for realizing high-efficiency and cost-effective solar cells.

RESULTS AND DISCUSSION

A schematic cross section of the surface textures used in this work is illustrated in Figure 1. We realized two thin free-standing absorbing slabs in c-Si wafers that were originally 300 μm thick. Both slabs had the same high aspect ratio b-Si FS texture, but the BS was either alkaline-textured with low aspect ratio random pyramids (textured BS) or just kept flat (flat BS). The b-Si FS texture was realized with a maskless reactive ion etching (RIE) process, which can be implemented in all commercially available dry etching tools. The thickness of the slabs was tuned by varying the etching time as described in the Methods section. We investigated a series of six pairs of slabs with different thicknesses. We measured the thickness of six slabs in the flat opening to be 190, 140, 100, 80, 40, and 28 μm, respectively. We also noticed that the standard alkaline etching process[23] for fabricating the pyramids generally reduced the corresponding thicknesses of slabs in the textured opening by more than 5 μm.

The atomic force microscopy (AFM) scans of b-Si texture, random pyramids, and the flat opening are illustrated in Figure 1a–c, respectively. The extracted root-mean-square roughness ($\sigma_{\rm rms}$) and correlation length ($L_{\rm c}$) of these three surfaces are reported in the inset table in Figure 1. Our b-Si FS texture exhibited an aspect ratio $\sigma_{\rm rms}/L_{\rm c}$ close to 0.37, while the random pyramids had a shallower aspect ratio close to 0.18. Finally, the surface of the flat opening was found to be virtually flat. As it will be shown later, by tuning the etching conditions for the b-Si FS texture, we achieved an extremely low broad-band reflectance. In addition, the b-Si FS texture led to an excellent light scattering inside the bulk. This aspect was confirmed before the fabrication of the BR by measuring the haze parameter of the slabs in transmittance ($H_{\rm T}$) with an integrating sphere (IS), where $H_{\rm T}$ is defined as the ratio between the diffused and the total transmittance. In the wavelength range between 400 and 1200 nm, a value of $H_{\rm T} \approx 1$ was found for both textured and flat BS configurations independently from the thickness of the slabs.

In standard commercial solar cells, a 70 nm thick SiN ARC layer is usually deposited via radiofrequency plasma-enhanced chemical vapor deposition (rf-PECVD) to provide electrical passivation and reduction of the front reflectance. However, when applied to the b-Si texture, SiN does not show good enough electrical passivation properties due to a poor surface coverage by rf-PECVD.[24] Instead, thermally grown dry SiO_2[21] and Al_2O_3 deposited via ALD[22] are more suitable for achieving good surface passivation of the b-Si. The drawbacks of these techniques, such as a high thermal budget or low deposition rate, are compensated by an excellent antireflective effect of the b-Si FS texture. In addition, because for b-Si FS texture there is no need of an additional ARC, a coating of a few tens of nanometers is sufficient to achieve reasonable surface passivation.[25] Once it was established that b-Si can be efficiently passivated, we focused on the rear side of our structured slabs to make a choice between SiO_2 and Al_2O_3. In fact, our light-trapping scheme was completed with an omnidirectional DBR in the role of dielectric BR, and its optical performance was compared with a reference 100 nm thick Ag BR. However, in order to carry out a fair comparison between the two types of BR, at least a 100 nm thick oxide layer was needed to reduce the metal absorption in the case of the metallic BR and thus enhance the internal reflectance.[12,27] To fulfill this requirement, we finally opted for thermally grown wet SiO_2, since its growth rate is faster than that of dry SiO_2 or Al_2O_3.

A 3-D Maxwell equations solver based on the finite element method[26] was used to design our dielectric DBR.[27,28] A DBR is formed by alternating dielectric layers with refractive index mismatch. Such a multilayer stack delivers high reflectance in a certain wavelength range around the so-called Bragg wavelength (λ_B). In the context of our work, the most stringent requirement for a DBR used as BR is to achieve $R_b = 1$ in the wavelength range of weak absorption of c-Si independently from the angle of incidence and the polarization of light. This is the so-called omnidirectionality.[28] This concept is of major importance in our light-trapping scheme. Since the b-Si FS texture demonstrates strong scattering properties leading to largely diffused light inside the absorber slab, the BR must provide the highest reflectance for all illumination conditions.

To design an omnidirectional dielectric DBR, two conditions have to be fulfilled: (i) the maximal refraction angle at the interface between the incident medium and the DBR must not exceed the Brewster angle at the internal interface of the first DBR pair and (ii) the DBR must exhibit a high reflectance in a selected wavelength range for all angles of incidence and for both polarizations.[28−30] In particular, when the first condition is not fulfilled, the electromagnetic field is partly transmitted throughout the dielectric reflector, which results in $R_b < 1$. The first condition can be mathematically expressed as follows:[31]

$$n_0' = \frac{n_H n_L}{\sqrt{{n_H}^2 + {n_L}^2}} > n_0 \tag{1}$$

where n_0, n_H, and n_L are the real part of the complex refractive index of the incident medium, high refractive index material, and low refractive index material, respectively. The first omnidirectionality condition is presented in Figure 2. Given the refractive index of the incident medium, one can choose the refractive indexes of materials that will constitute the DBR in such a way that their combination n_0' is greater than n_0. We designed our DBR around the band gap of c-Si with $\lambda_B = 1000$ nm. Setting SiO_2 as incident medium, a-Si:H (n_H) and a-SiN_x:H (n_L) were considered good candidates for constituting our dielectric DBR. Their refractive indexes at λ_B satisfied the first omnidirectionality condition ($n_0' = 1.58 > n_0 = 1.5$), and their thickness in the DBR was determined as $d_{H(L)} = \lambda_B/4n_{H(L)}$, with $d_{H(L)}$ the thickness of a-Si:H (a-SiN_x:H).[28]

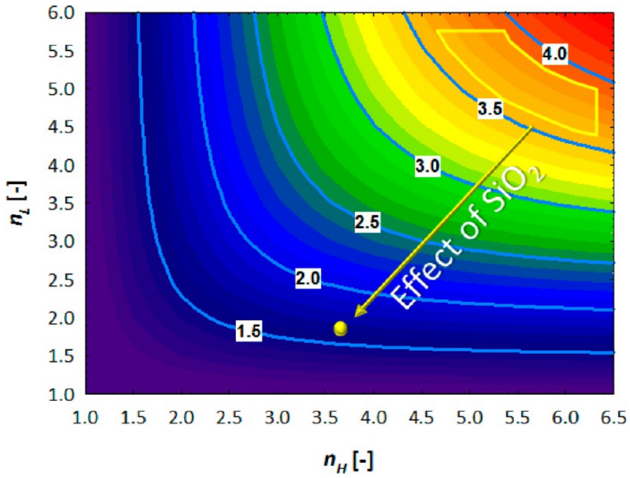

Figure 2. Contour plot depicting the first omnidirectionality condition: $n_0' > n_0$ (eq 1). Light blue lines on the contour plot are the isovalue curves indicating the refractive index of the incident medium (n_0) on top of the DBR. To fulfill this condition for a DBR ($n_0' = f(n_L,n_H)$) having bulk c-Si as incident medium (n_0) (see yellow area), nonabsorbing materials with high n_L and n_H refractive indexes at $\lambda_B = 1000$ nm are required. Their fabrication is however not trivial. Instead, considering a SiO_2 layer ($n_0 = n_{SiO2(1000\ nm)} = 1.5$) between the bulk c-Si and DBR allows for the use of existing nonabsorbing materials, $\lambda_B = 1000$ nm, such as a-SiN_x:H ($n_L = n_{a\text{-}SiNx(1000\ nm)} = 1.76$, $d_{a\text{-}SiNx} = 146$ nm) and a-Si:H ($n_H = n_{a\text{-}Si:H(1000\ nm)} = 3.61$, $d_{a\text{-}Si:H} = 69$ nm).

Optical simulations of a flat stack of c-Si (half space)/SiO_2 (100 nm)/DBR, depicted in Figure 3a, were carried out. The aim of these simulations was to find a minimum number of a-Si:H/a-SiN_x:H pairs that results in $R_b = 1$ and fulfills the second omnidirectionality condition. As Figure 3b shows, both requirements are met using six pairs of a-Si:H (69 nm)/a-SiN_x:H (146 nm). This number of pairs represents a good compromise between processing time of the DBR and high internal rear reflectance. In Figure 3b the theoretical angle-dependent Bragg wavelength (λ_B) and the right and left photonic band gap edges (λ_L and λ_R, respectively) are also depicted. It is noticeable that the results of our optical modeling using materials with wavelength-dependent properties were close to the theory.[28] The typical quenching of λ_R in P-polarization due to the Brewster angle was reproduced as well. These optical simulations rigorously describe the internal rear reflectance in our ultrathin c-Si slabs coated with dielectric DBR at the flat BS. On the other hand, considering the textured BS, we expect some deviation in the internal rear reflectance, as the simulated thicknesses can be realized in practice only on a flat surface. A cross-sectional scanning electron microscopy (SEM) image of the 20 μm thick textured and 28 μm flat c-Si slabs with dielectric omnidirectional DBR are shown in Figure 4a and b, respectively. The b-Si FS texture (green inset) is the same for both BS configurations. Random pyramidal BS texture conformally coated by the designed DBR is clearly visible on the 20 μm thick bulk c-Si (red inset in Figure 4a). Analyzing these images, we found that the morphology of b-Si texture is characterized by conical shapes having a radius around 250 nm and a height lower than 1 μm. These values are in reasonable agreement with the results obtained from the AFM technique.

All fabricated slabs in both BS configurations and with different BRs were optically characterized by measuring the reflectance and transmittance (R and T) in the wavelength

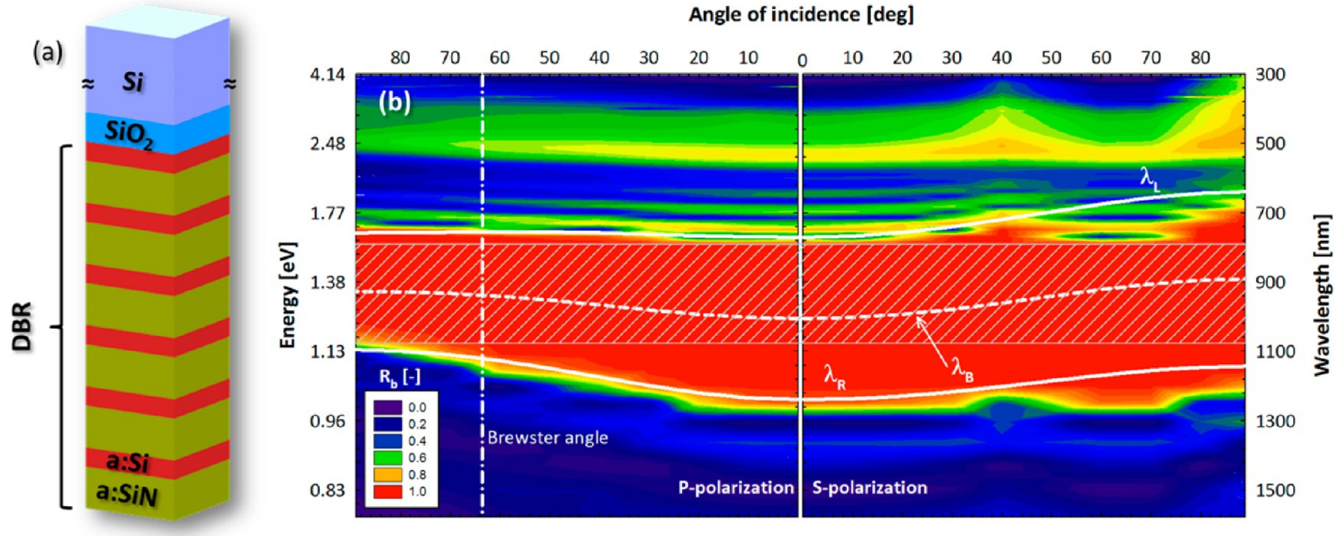

Figure 3. (a) Simulated structure and (b) calculated internal reflectance for different angles of incidence and for P-polarization (left) and S-polarization (right). The gray shaded area represents the omnidirectional photonic band gap (second omnidirectional condition). The white horizontal solid and dashed curves are the theoretical angle-dependent photonic band edges (λ_L and λ_R) and the Bragg wavelength, respectively. For angle of incidence 0°, λ_B is equal to 1000 nm. λ_L and λ_R, theoretically calculated[28] for wavelength-independent $n_L = 1.76$ and $n_H = 3.61$, closely follow the region of high reflectance in both polarizations. In the P-polarization panel, the vertical dash-dotted line locates the Brewster angle of the optical system. The colors from violet to red represent the increasing value of the rear internal reflectance R_b for both polarizations.

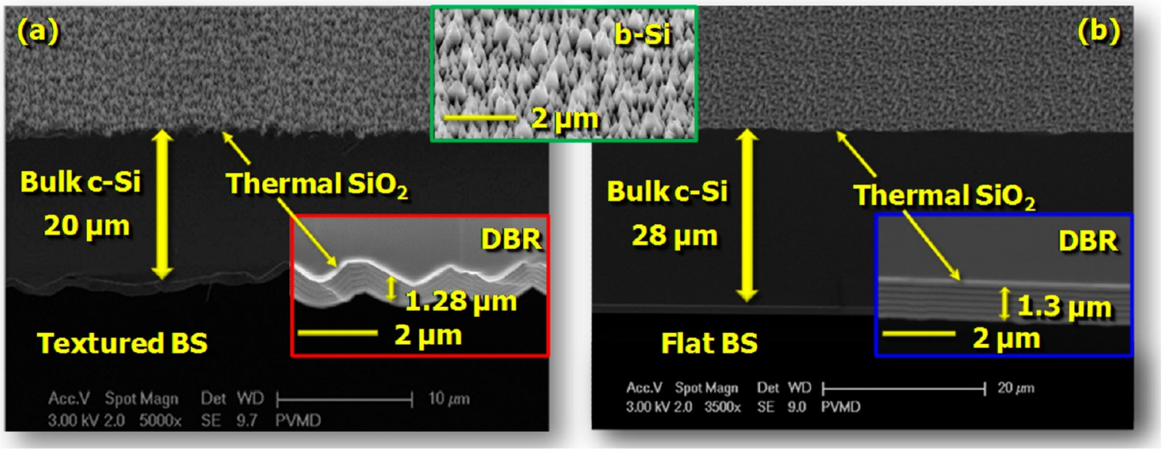

Figure 4. Cross-sectional SEM images of (a) 20 μm thick absorber with textured BS and (b) 28 μm thick absorber with flat BS. The three colored insets show a close-up of the common front nanotexture coated with thermal SiO_2 (green) and of the textured (red) and the flat (blue) BS coated with thermal SiO_2 and six pairs of a-Si:H/a-SiN_x:H conformal DBR. All SEM images were taken at a tilt angle of 45°.

range between 400 and 1200 nm using the IS. Total absorptance (A_{tot}) was calculated as $A_{tot} = 1 - R - T$. This quantity corresponds to the absorptance in silicon (A_{si}) only when the BR is constituted by nonabsorbing materials. On the other hand, in case of metallic BR the measured A_{tot} includes also the absorption in the metal layer. To compare only A_{si} for both BR configurations, we used our analytical model that is capable of distinguishing A_{si} from A_{tot}[32] (see Methods section, eq 4). The experimentally determined A_{Si} were therefore compared with absorptances calculated from the $4n^2$ classical absorption limit (A_{4n2}) and the single pass limit (A_{SP}):[10]

$$A_{4n^2} = 1 - \frac{1}{1 + 4{n_{Si}}^2 \alpha_{Si} d} \tag{2}$$

$$A_{SP} = 1 - e^{-\alpha_{Si} d} \tag{3}$$

where n_{Si} and α_{Si} are the real part of the complex refractive index and the absorption coefficient of c-Si, respectively.

The measured A_{si} of a 20 μm (28 μm) thick c-Si slab in the case of the b-Si FS texture and alkaline-textured (flat) BS coated with either dielectric DBR or reference Ag are reported in Figure 5a and b, respectively. Considering both figures, it is clear that the absorptance in our nanotextured c-Si wafers for both BRs is much higher than that calculated according to the single pass limit. This highlights the goodness of the scattering properties of the developed nanotexturing. However, the texturing of the BS with random pyramids introduces an additional level of scattering, which eventually enhances the NIR response. Even though the front b-Si nanotexture achieves an excellent broad-band antireflective effect at the air/silicon front interface, we speculate that it may not actuate a Lambertian scattering inside the c-Si absorbers. In this respect, we recognize that further work has to be done from the

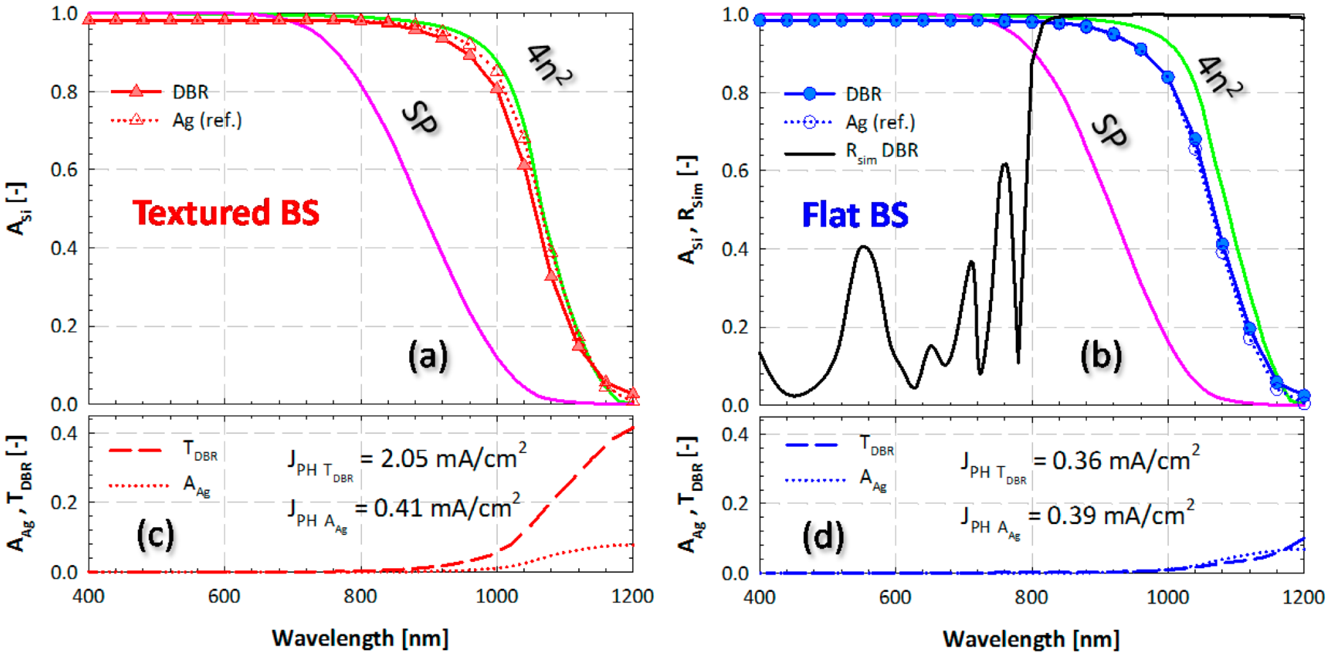

Figure 5. Measured absorptances in the case of the b-Si FS texture and (a) 20 μm thick c-Si absorber with the alkaline textured BS or (b) 28 μm thick c-Si absorber with the flat BS. In both figures the absorptances of silicon with the optimized dielectric DBR and the reference 100 nm thick Ag layer BRs are reported. Absorptances are compared with the $4n^2$ classical absorption limit and single pass absorption (green and pink curves, respectively). Black line in (b) shows the simulated internal rear reflectance in c-Si with the optimized DBR. This spectrum corresponds to perpendicular incidence (0°) and was extracted from Figure 3. Panels (c) and (d) show the optical losses related to the Ag absorptance (calculated) in the case of metallic BR and transmittance (measured) in the case of dielectric DBR for textured and flat BS, respectively. The implied photocurrent densities of such optical losses were calculated according to eq 5 of the Methods section, using A_{Ag} (calculated) or T_{DBR} (measured) in place of A_{Si}.

perspective of angular intensity distribution[33] obtained by front b-Si nanotexture inside the c-Si absorbers.

Integrating the measured absorptance spectra of all our structured absorber slabs with the reference solar photon flux in the wavelength range between 400 and 1200 nm (see Methods section, eq 7), we could calculate the so-called implied J_{PH}. Considering the thickness of the realized slabs and operating the same calculation in the identical wavelength range but using either A_{4n2} or A_{SP}, we could also carry out the implied J_{PH} of the $4n^2$ classical absorption limit and of the single pass limit. In particular, in the case of a 20 μm thick c-Si slab with textured BS, we achieved 99% and 99.8% of the implied J_{PH} of the theoretical $4n^2$ classical absorption limit with dielectric and metallic BR, respectively. To our knowledge, this is so far the closest experimental evidence of the $4n^2$ classical absorption limit.

In Figure 5b the simulated internal reflectance for the flat BS coated with DBR is also reported. The designed wavelength range of high internal reflectance of the DBR (800−1200 nm) perfectly matches the weak-absorption region of c-Si. However, in the case of even thinner wafers, the limited bandwidth of the DBR would lead to a decrease of the optical absorption already in the red response. To overcome such a limitation, a modulated DBR can be used to achieve broader bandwidth.[28,34]

The slab with the dielectric DBR on flat BS shows slightly higher absorptance compared with the reference Ag BR. The opposite outcome is observed in the case of our record slab with textured BS. To explain this behavior, we looked at the spectral losses of the two BRs in both BS configurations and calculated their implied J_{PH}. The spectral losses are due to the calculated optical absorption in the metallic layer (Ag BR) or the measured transmittance through the dielectric stack (DBR BR). The DBR is optimized for flat interfaces, and therefore it shows slightly lower optical losses than Ag BR in the case of flat BS as presented in Figure 5d. Instead, in the case of textured BS (see Figure 5c), our DBR design suffers from higher optical losses with respect to Ag BR, not being optimized for textured interfaces. This setback was found to be independent from the absorber thickness, as depicted in Figure 6a,b.

On the other hand, still looking at Figure 6a,b, what was found to be thickness dependent was the gap between the J_{PH}

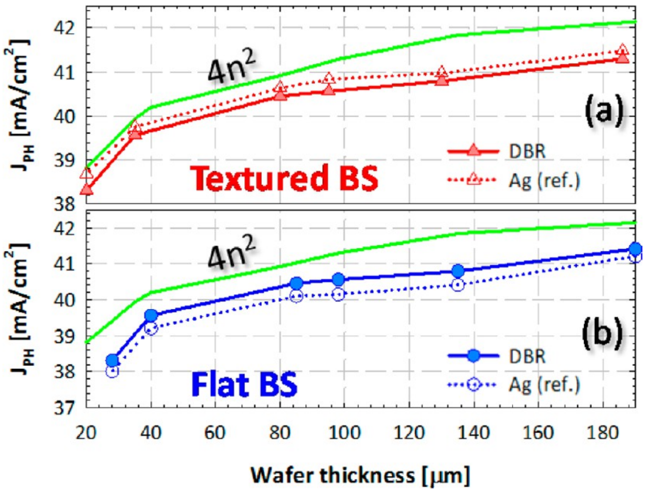

Figure 6. J_{PH} calculated between 400 and 1200 nm for AM1.5 illumination conditions and different absorber thicknesses in the case of (a) textured and (b) flat BS (see eq 5 in the Methods section). The BS is coated either with DBR or with the reference Ag BR.

predicted by the $4n^2$ limit and the one calculated from the measured absorptances. In the case of textured BS, such a gap clearly decreases for thinner absorbers endowed with both BRs. Instead, in the case of flat BS, such a trend is less evident, as the gap for both BRs decreases at a slower pace. Either way, in our samples with textured BS the gap reduced to 1% or less for absorber thicknesses smaller than 35 μm. This thickness seems be a threshold below which the additional scattering effect introduced by the rear random pyramids eventually starts to support the nonideal Lambertian scattering in the c-Si absorber given by the front nanotexture. The fact that the gap monotonically decreases for smaller absorber thicknesses could be related to an enhanced photon absorption at long wavelengths due to a better coupling of the electromagnetic field with diffraction modes introduced by the back side scattering, as illustrated in recent simulation results.[35,36]

The implied J_{PH} determined for a double-sided textured wafer coated with Ag BR with thicknesses equal to or less than 35 μm approached the J_{PH} predicted by the $4n^2$ limit as reported in Figure 6a. We believe that a similar result can be achieved on thin c-Si wafers with a DBR optimized for textured BS. Therefore, further simulations studies are required to find the optimum DBR design on textured BS that can outperform the metallic BR. Considering the implied J_{PH} based on the absorptance spectra of 100 μm and 135 μm thick absorbers, we did not approach the $4n^2$ absorption limit. However it is noticeable that we obtained at least a 1 mA/cm^2 higher J_{PH} value with respect to state-of-the-art c-Si solar cells having comparable bulk thickness.[37−40]

Finally, we want to discuss the embedding of our light-trapping scheme in next-generation c-Si solar devices. Figure 7a shows the 20 μm thick c-Si absorber slab extracted from the c-Si wafer support. Such a slab is flexible and can be processed to fabricate an ultrathin solar cell. Although our process flow involved a photolithographic step (see Methods section), mostly required for mechanical support and quality control over pairs of slabs, our light-trapping scheme may be straightforwardly implemented at an industrial level with maskless processes. In our vision, the solar cell technology that would take the highest efficiency gain from our light-trapping scheme is the one adopted by Sunpower,[41,42] as sketched in Figure 7b. The main feature of such a technology is the fabrication of both contacts at the BS of the device. These contacts are usually arranged in an interdigitated fashion, the so-called interdigitated back contacted design (IBC). With this type of solar cell technology, since no metal−Si contact is required at the FS (i.e., no metal front grid) and a lightly doped floating front emitter is usually employed,[43] both low front surface recombination and parasitic emitter absorption in the blue region can be expected. For these reasons, the excellent broad-band antireflective effect provided by our front nano-texturing could be fully exploited on the entire solar device area. It is clear that state-of-the-art passivation of FS of our c-Si ultrathin absorbers must be preliminarily actuated in order to fabricate the solar device sketched in Figure 7b. In a future publication we shall present our improved passivation of b-Si nanotexturing using SiO_2 and Al_2O_3 with a surface treatment after RIE aiming to increase minority carrier lifetime.[21]

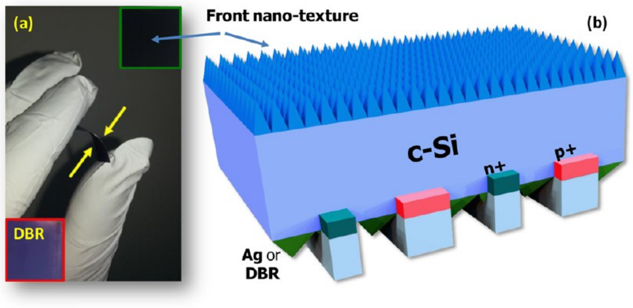

Figure 7. (a) Photo of 20 μm thick flexible silicon absorber extracted from the c-Si wafer support. Top-right and bottom-left photos indicate the b-Si front surface and the rear random pyramids coated with DBR, respectively. (b) Our vision: to apply the presented light-trapping scheme in IBC c-Si solar cell technology.

■ CONCLUSIONS

We presented an advanced light-trapping scheme based on b-Si FS texture, random pyramid BS texture, and dielectric DBR. After designing a dielectric omnidirectional DBR for flat BR, we realized ultrathin textured c-Si slabs having thicknesses in the range between 190 and 20 μm. We measured c-Si absorptance spectra that, integrated between 400 and 1200 nm with the reference solar photon flux, resulted in implied J_{PH} up to 99.8% of the maximal theoretical one calculated for the same wavelength range and wafer thickness. To our knowledge this is the closest experimental evidence of the $4n^2$ classical absorption limit in c-Si. Further studies should aim at the fabrication of an optimized dielectric DBR that suffers less from transmittance losses in the region of weak absorption of c-Si when deposited on a textured surface. Additionally, the angle dependence of light scattering given by the front nanotexture inside the c-Si absorber should be addressed. This is to pursue an even better antireflective front texture, which allows an implied J_{PH} near the $4n^2$ absorption limit with flat BS. We believe that high-efficiency, ultrathin solar cells can be fabricated once that the presented light-trapping scheme is well passivated electrically. This can be achieved by combining a SiO_2- or Al_2O_3-based passivation with a surface treatment after RIE, aiming to increase minority carrier lifetime.[21] Finally, the IBC approach was indicated as the most suited technology in order to fully exploit the optical advantages brought by our light-trapping scheme.

■ METHODS

Process Flow Description. We used 4 in. CZ p-type Si wafers with initial thickness 300 ± 5 μm and resistivity >1000 Ω·cm. The front b-Si texture was made by RIE using a gaseous mixture of SF_6 and O_2 (see Figure 1a). This texturing process can be realized also on n-type Si wafers. After standard cleaning, rinsing, and drying of the substrates, SiN was deposited on both sides of the wafers in a tube furnace by means of low-pressure chemical vapor deposition (LP-CVD). On the nontextured side of the wafers, a photolithographic step was performed to create two openings, each measuring 3×3 cm^2 in area. In such openings the SiN layer was dry-etched in a C_2F_6 plasma for 20 s. After that the photoresist outside the openings was dry-etched in a O_2 plasma for 5 min (Europlasma stripper), and the silicon bulk in the two openings was thinned in a bath of KOH at 80 °C characterized by an etching rate of 100 μm/h. Tuning the etching time, we could fabricate two c-Si slabs in each of the six different c-Si wafers. We measured the thickness of the slabs by means of a Veeco Dektak 150 profilometer, obtaining in

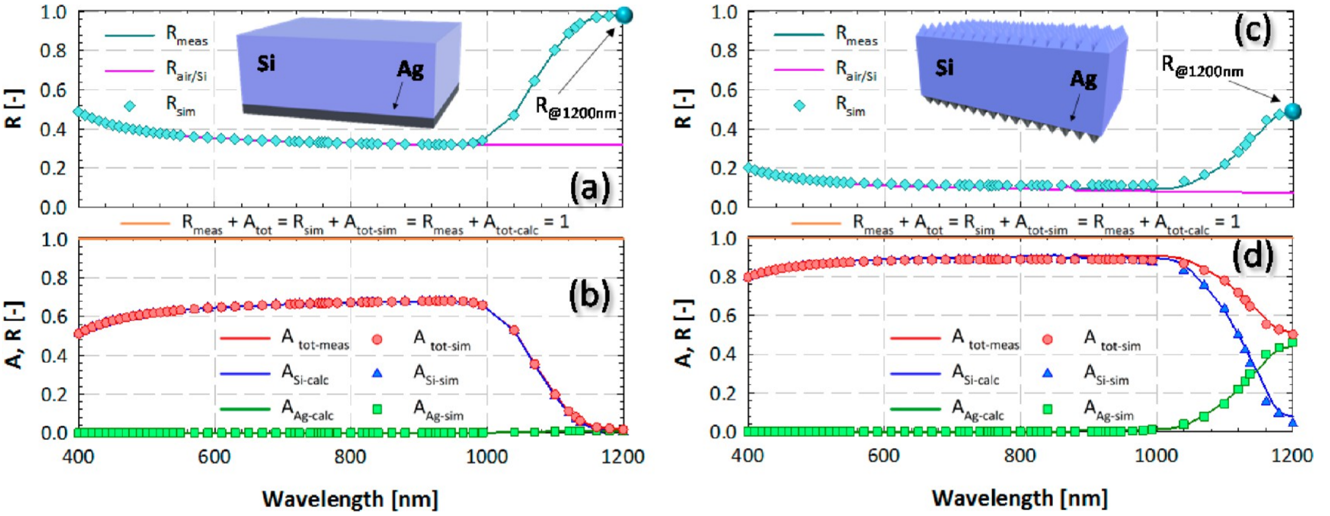

Figure 8. (a−c) R_{meas}, $R_{air/Si}$, and R_{sim} for a 280 μm thick wafer coated on one side with 100 nm thick Ag back reflector in (a) flat and (c) pyramidally textured configurations. The fabricated/simulated structures are sketched in the insets. (b−d) $A_{Si\text{-}cal}$ and $A_{Ag\text{-}cal}$ calculated from eqs 4 and 6, respectively, and superposed to simulated $A_{Si\text{-}sim}$ and $A_{Ag\text{-}sim}$ for the respective structures illustrated in the top insets. Also A_{tot} and $A_{tot\text{-}sim}$ spectra are here reported. For both structures, the energy conservation ($R_{meas} + A_{tot} = R_{sim} + A_{tot\text{-}sim} = R_{meas} + A_{tot\text{-}calc} = 1$) is verified (orange line).

each pair of openings 190, 135, 100, 80, 40, and 28 μm thick bulk c-Si, respectively. For each wafer, one of the openings was further etched in a TMAH-IPA alkaline bath to get a texture characterized by random pyramids (textured BS, see Figure 1b), while the other opening was kept flat by using AI Technology spin-coated thinning wax as a protective layer resistant to the alkaline solution (flat BS, see Figure 1c). It should be noted that TMAH-IPA texturing in the textured opening reduces the Si thickness by more than 5 μm with respect to the flat opening. The protective thinning wax layer was later etched in acetone at room temperature for 2 min. At this point, the LP-CVD SiN, still present on the front of b-Si and on the rear side outside the openings, was etched from all samples in a H_3PO_4 solution (85 wt % diluted in H_2O) at 157 °C for 42 min. A wet thermal SiO_2 layer of 100 nm was grown on both sides of the wafers at 1100 °C in a tube furnace. To be able to compare the performance of the dielectric DBR with that of a reference metallic BR using the same front/rear textured c-Si slabs, we first coated the rear side of the slabs with a 100 nm thick Ag layer (reference metallic BR) using physical vapor deposition in a Provac PRO500S. After the optical characterization of the samples (see the next section), we removed the metallic BR in a HNO_3 solution (69.5% diluted in H_2O) at room temperature for 30 s, which left untouched c-Si and SiO_2. Finally, the dielectric DBR was fabricated by depositing six a-Si:H/a-SiN_x:H pairs using SiH_4 and SiH_4 + NH_3 plasmas in an rf-PECVD AMIGO Elettrorava cluster tool.

Sample Characterization. The morphological analysis of the samples was performed with AFM using an NT-MDT nTegra setup. Extracted values of σ_{rms} and L_C are reported in the inset table of Figure 1. For the visual investigation of the surface textures, the thickness of c-Si textured slabs, and the composition of the DBR, a Philips XL-150 SEM was used (see Figure 4b). Wavelength-dependent complex refractive indexes of a-SiN_x:H, a-Si:H, and SiO_2 were extracted from ellipsometry spectra using a J. A. Wollam Co. M-2000DI spectroscopic ellipsometer. At the design wavelength of our dielectric DBR (λ_B = 1000 nm), the real parts of the complex refractive indexes of a-SiN_x:H, a-Si:H, and SiO_2 were 1.76, 3.67, and 1.5, respectively. Reflectance (R) and transmittance (T) of passivated FS/BS textured c-Si slabs with and without metallic BR or dielectric DBR were measured using an IS accessory mounted on a PerkinElmer Lambda 950 spectrophotometer in the wavelength range between 400 and 1200 nm.

Optical Modeling and Implied Photogenerated Current Density. In an opaque optical system such as a c-Si/Ag stack, we developed an empirical model[32] for which the absorptance in silicon can be calculated as

$$A_{Si\text{-}calc} = \frac{R_{air/Si}(1 - R_{@1200nm}) - R_{meas} + R_{@1200nm}}{R_{@1200nm}} \tag{4}$$

where R_{meas} is the measured total reflectance, $R_{@1200\ nm}$ is R_{meas}(1200 nm), and $R_{air/Si}$ is the contribution of reflected light bouncing inside the bulk c-Si at the air/Si interface, estimated by linearly extrapolating R_{meas} between 700−900 and 1200 nm. Measuring the total reflectance of an opaque optical system (i.e., no transmittance) such as c-Si/Ag means identifying also the total absorptance (A_{tot}), which is given by the sum of the absorptance spectra of c-Si (A_{Si}) and Ag (A_{Ag}):

$$A_{tot} = A_{Si} + A_{Ag} = 1 - R_{meas} \Rightarrow A_{Ag} = 1 - R_{meas} - A_{Si} \tag{5}$$

Thus, using only R_{meas} and eq 4, it is possible to distinguish for this type of optical system A_{Si} from A_{Ag}. To verify eq 4, we apply a three-step procedure. Even though we tested our empirical model in several opaque optical systems and for different absorber thicknesses, the validation of this model is reported here for the optical system c-Si (280 μm)/Ag (100 nm) in both flat and pyramidally textured configurations. In the first step, we match measured R_{meas} and A_{tot} with the corresponding R_{sim} and $A_{tot\text{-}sim}$ using the optoelectrical simulator Advanced Semiconductor Analysis (ASA) software.[32,44,45] By achieving this goal, the software provides the absorptance spectra in c-Si ($A_{Si\text{-}sim}$) and in Ag ($A_{Ag\text{-}sim}$) such that $A_{tot\text{-}sim} = A_{Si\text{-}sim} + A_{Ag\text{-}sim}$. In the second step, we calculate the absorptance spectrum in c-Si ($A_{Si\text{-}calc}$) according to eq 4, and we compare this calculated spectrum with $A_{Si\text{-}sim}$. After that we calculate the absorptance spectrum in Ag ($A_{Ag\text{-}calc}$) from

$$A_{\text{Ag-calc}} = 1 - R_{\text{meas}} - A_{\text{Si-calc}} \tag{6}$$

Finally, in the third step, we sum up R_{meas}, $A_{\text{Si-calc}}$, and $A_{\text{Ag-calc}}$ (i.e., $R_{\text{meas}} + A_{\text{tot-calc}}$) aiming to observe 1 $\forall\lambda$, as it would be in the case of $R_{\text{meas}} + A_{\text{tot}}$ (see Figure 8).

The implied photocurrent density (J_{PH}) of absorptance in textured c-Si slabs was calculated as follows:

$$J_{\text{PH}} = -q\int_{\lambda_1}^{\lambda_2} A_{\text{Si}}(\lambda)\, \Phi_{\text{AM1.5}}(\lambda)\, \mathrm{d}\lambda \tag{7}$$

where q is the elementary charge, A_{Si} is the absorptance of silicon, $\Phi_{\text{AM 1.5}}$ is the standard $\text{AM}_{1.5}$ photon flux,[46] and $[\lambda_1, \lambda_2]$ is the wavelength range of interest.

AUTHOR INFORMATION

Corresponding Author

*E-mail: a.ingenito@tudelft.nl, o.isabella@tudelft.nl, m.zeman@tudelft.nl. Fax: +31 15 27 82968.

Author Contributions

A.I. conceived the light-trapping scheme, conducted the experiments and the measurements, wrote the manuscript, and composed the graphical material. A.I. and O.I. designed the dielectric DBR. O.I. carried out the optical simulations and added supporting graphical material. O.I. and M.Z. supervised the work and proofread the manuscript.

Notes

The authors declare no competing financial interest.

ACKNOWLEDGMENTS

The authors thank M. Tijssen (TU Delft) for help with the deposition of dielectric DBR, R. A. Vasudevan (TU Delft) for support with extraction of optical properties from ellipsometry spectra, Fai Tong Si and Dimitris Deligiannis for preparing samples used in the Methods section, Delft Institute of Microsystems and Nanoelectronics (DIMES, TUDelft) for facility services, and Dr. A. Poruba (SolarTec) for useful discussions. This work was carried out with a subsidy from the Dutch Ministry of Economic Affairs under the EOS-LT program (Project No. EOSLT10037).

REFERENCES

(1) Zhao, J.; Wang, A.; Altermatt, P.; Green, M. A. 24% efficient silicon solar cells with double layer antireflection coatings and reduced resistance loss. *Appl. Phys. Lett.* **1995**, *66*, 3636−3638.

(2) Jäger-Waldau, A. *PV Status Report 2012*; Joint Research Centre, Institute for Energy and Transport, 2012.

(3) del Cañizo, C.; del Coso, G.; Sinke, W. C. Crystalline silicon solar module technology: towards the 1 € per watt-peak goal. *Prog. Photovolt Res. Appl.* **2008**, *17*, 199−209.

(4) Goodrich, A.; Hacke, P.; Wang, Q.; Sopori, B.; Margolis, R.; James, T. L.; Woodhouse, M. A wafer-based monocrystalline silicon photovoltaics road map: utilizing known technology improvement opportunities for further reductions in manufacturing costs. *Sol. Energy Mater. Sol.* **2013**, *114*, 110−135.

(5) Micciche, B.; Dingle, B. Understanding the causes for cell breakage during the cell interconnecting process−part I. *Proceedings of the 21st European Photovoltaic Solar Energy Conference*; 2006.

(6) Munzer, K. A.; Holdermann, K. T.; Schlosser, R. E.; Sterk, S. Thin monocrystalline silicon solar cells. *IEEE Trans. Electron Devices* **1999**, *46*, 2055−2061.

(7) Glunz, S. W.; Rein, S.; Warta, W.; Knobloch, J.; Wettling, W. On the degradation of Cz-silicon solar cells. *Proceedings of the 2nd World Conference on Photovoltaic Energy Conversion*; 1998; pp 1343−1346.

(8) Kray, D.; Kampwerth, H.; Schneiderlochner, E. Comprehensive experimental study on the performance of very thin laser-fired high-efficiency solar cells. *Proceedings of the 19th European Photovoltaic Solar Energy Conference*; 2004; pp 608−611.

(9) Green, M. A. *Silicon Solar Cells: Advanced Principles & Practice*; Centre for Photovoltaic Devices and Systems, University of New South Wales, 1995.

(10) Tiedje, T.; Yablonovitch, E.; Cody, G. D.; Brooks, B. G. Limiting efficiency of silicon solar cells. *IEEE Trans. Electron Devices* **1984**, *31*, 711−716.

(11) Campbell, P.; Green, M. A. Light trapping properties of pyramidally textured surfaces. *J. Appl. Phys.* **1987**, *62*, 243.

(12) Holman, Z. C.; Filipič, M.; Lipovšek, B.; De Wolf, S.; Smole, F.; Topič, M.; Ballif, C. Parasitic absorption in the rear reflector of a silicon solar cell: simulation and measurement of the sub-bandgap reflectance for common dielectric/metal reflectors. *Sol. Energy Mater. Sol.* **2014**, *120*, 426−430.

(13) Wang, K. X.; Yu, Z.; Liu, V.; Cui, Y.; Fan, S. Absorption enhancement in ultrathin crystalline silicon solar cells with antireflection and light-trapping nanocone gratings. *Nano Lett.* **2012**, *12*, 1616−1619.

(14) Garnett, E.; Yang, P. Light trapping in silicon nanowire solar cells. *Nano Lett.* **2010**, *10*, 1082−1087.

(15) Cao, L.; Fan, P.; Vasudev, A. P.; White, J. S.; Yu, Z.; Cai, W.; Schuller, J. A.; Fan, S.; Brongersma, M. Semiconductor nanowire optical antenna solar absorbers. *Nano Lett.* **2010**, *10*, 439−445.

(16) Battaglia, C.; Boccard, M.; Haug, F.-J.; Ballif, C. Light trapping in solar cells: when does a Lambertian scatterer scatter Lambertianly? *J. Appl. Phys.* **2012**, *112*, 094504.

(17) Isabella, O.; Ingenito, A.; Linssen, D.; Zeman M. Front/rear decoupled texturing in refractive and diffractive regimes for ultra-thin silicon-based solar cells. *Renewable Energy and the Environment, OSA Technical Digest*; **2013**, paper PM4C.2.

(18) Wang, S.; Weil, B.; Li, Y.; Wang, K. X.; Garnett, E.; Fan, S.; Cui, Y. Large Area Free-Standing Ultrathin Single-Crystal Silicon as Processable Materials. *Nano Lett.* **2013**, *13*, 4393−4398.

(19) Zeng, L.; Yi, Y.; Hong, C.; Liu, J.; Feng, N.; Duan, X.; Kimerling, L. C.; Alamariu, B. A. Efficiency enhancement in Si solar cells by textured photonic crystal BR. *Appl. Phys. Lett.* **2006**, *89*, 111111.

(20) Isabella, O.; Dobrovolskiy, S.; Kroon, G. A.; Zeman, M. Design and application of dielectric distributed Bragg back reflector in thin-film silicon solar cells. *J. Non-Cryst. Solids* **2012**, *358*, 2295−2298.

(21) Oh, J.; Yuan, H. C.; Branz, H. M. An 18.2%-efficient black-silicon solar cell achieved through control of carrier recombination in nanostructures. *Nat. Nanotechnol.* **2012**, *7*, 743−748.

(22) Otto, M.; Kroll, M.; Käsebier, T.; Salzer, R.; Tünnermann, A.; Wehrspohn, R. B. Extremely low surface recombination velocities in black silicon passivated by atomic layer deposition. *Appl. Phys. Lett.* **2012**, *100*, 191603.

(23) Papet, P.; Nichiporuk, O.; Kaminski, A.; Rozier, Y.; Kraiem, J.; Lelievre, J.-F.; Chaumartin, A.; Fave, A.; Lemiti, M. Pyramidal texturing of silicon solar cell with TMAH chemical anisotropic etching. *Sol. Energy Mater. Sol.* **2006**, *90*, 2319−2328.

(24) Kroll, M.; Otto, M.; Käsebier, T.; Füchsel, K.; Wehrspohn, R.; Kley, E.; Tünnermann, A.; Pertsch, T. Black silicon for solar cell applications. *Proc. SPIE 8438, Photonics Solar Energy Syst. IV* **2012**, 843817.

(25) Hoex, B.; Heil, S. B. S.; Langereis, E.; van de Sanden, M. C. M.; Kessels, W. M. M. Ultralow surface recombination of c-Si substrates passivated by plasma-assisted atomic layer deposited Al_2O_3. *Appl. Phys. Lett.* **2006**, *89*, 042112.

(26) White papers in Ansys HFSS official website, http://www.ansoft.com/products/hf/hfss/.

(27) Kray, D.; Hermle, M.; Glunz, S. W. Theory and experiments on the back side reflectance of silicon wafer solar cells. *Prog. Photovolt: Res. Appl.* **2007**, *16*, 1−15.

(28) Isabella, O. Light management in thin-film silicon solar cells. Ph.D. dissertation, 2013.

(29) Fink, Y.; Winn, J. N.; Fan, S.; Chen, C.; Michel, J.; Joannopoulos, J. D.; Thomas, E. L. A dielectric omnidirectional reflector. *Science* **1998**, *282* (5394), 1679−1682.

(30) Chigrin, D. N.; Lavrinenko, A. V.; Yarotsky, D. A.; Gaponenko, S. V. Observation of total omnidirectional reflection from a one-dimensional dielectric lattice. *Appl. Phys.* **1999**, *68*, 25−28.

(31) Orfanidis, J. S. *Electromagnetic Waves and Antennas*; Rutgers University, 2010.

(32) Ingenito, A.; Isabella, O.; Zeman, M. Opto-electronic evaluation of thin double-textured crystalline silicon wafers. *39th IEEE Photovoltaic Specialist Conference*; 2013.

(33) Jäger, K.; Isabella, O.; van Swaaij, R. A. C. M. M.; Zeman, M. Angular resolved scattering measurements of nano-textured substrates in a broad wavelength range, *Meas. Sci. Technol.* **2010**, *22*, 10.1088/0957-0233/22/10/105601.

(34) Krč, J.; Zeman, M.; Luxembourg, S. L.; Topič, M. Modulated photonic-crystal structures as broadband back reflectors in thin-film solar cells, *Appl. Phys. Lett.* **2009**, *94*, 10.1063/1.3109781.

(35) Bermel, P.; Luo, C.; Zeng, L.; Kimerling, L.; Joannopoulos, J. Improving thin-film crystalline silicon solar cell efficiencies with photonic crystals. *Opt. Express* **2007**, *15*, 16986−17000.

(36) Biswas, R.; Xu, C. Nano-crystalline silicon solar cell architecture with absorption at the classical $4n^2$ limit. *Opt. Express* **2011**, *19*, A664−A672.

(37) Kinoshita, T.; Fujishima, D.; Yano, A.; Ogane, A.; Tohoda, S.; Matsuyama, K.; Nakamura, Y.; Tokuoka, N.; Kanno, H.; Sakata, H.; Taguchi, M.; Maruyama, E. The approaches for high efficiency HIT solar cell with very thin (<100mm) silicon wafer over 23%. *Proceedings of the 26th European Photovoltaic Solar Energy Conference*; 2011; Hamburg, Germany.

(38) Cousins, P. J.; Smith, D. D.; Luan, H.-C.; Manning, J.; Dennis, T. D.; Waldhauer, A.; Wilson, K. E.; Harley, G.; Mulligan, W. P. Generation 3: improved performance at lower cost. *Proceedings of the 35th Photovoltaic Specialists Conference*; 2010; pp 275−278.

(39) Swanson, D. *Solar Energy Mini-Series: The Silicon Photovoltaic Roadmap*; Stanford University, 2011, http://energyseminar.stanford.edu/sites/all/files/eventpdf/11-11-14%20Swanson.pdf.

(40) Green, M. A.; Emery, K.; Hishikawa, Y.; Warta, W.; Dunlop, E. D. Solar cell efficiency tables (version 41). *Prog. Photovolt: Res. Appl.* **2013**, *21*.

(41) Swanson, R. M. Device physics for backside-contact solar cells. *Proceedings of the 33rd IEEE Photovoltaic Specialists Conference*; San Diego, CA, USA, 2008.

(42) http://us.sunpowercorp.com/homes/.

(43) Ohrdes, T.; Römer, U.; Larionova, Y.; Peibst, R.; Altermatt, P. P.; Harder, N.-P. High fill-factors of back-junction solar cells without front surface field diffusion. *Proceedings of the 27th European Photovoltaic Solar Energy Conference*; 2012; pp 866−869

(44) Isabella, O.; Sai, H.; Kondo, M.; Zeman, M. Full-wave optoelectrical modeling of optimized flattened light-scattering substrate for high efficiency thin-film silicon solar cells. *Prog. Photovolt: Res. Appl.* **2012**, DOI: 10.1002/pip.2314.

(45) Zeman, M.; Isabella, O.; Solntsev, S.; Jäger, K. Modelling of thin-film silicon solar cells. *Sol. Energ. Mat. Sol.* **2013**, DOI: 10.1016/j.solmat.2013.05.037.

(46) http://rredc.nrel.gov/solar/spectra/am1.5/.